Biophysical Journal
Article

Biophysical Society

On the Origin of Microtubules' High-Pressure Sensitivity

Mimi Gao,[1] Melanie Berghaus,[1] Simone Möbitz,[1] Vitor Schuabb,[1] Nelli Erwin,[1] Marius Herzog,[1] Karin Julius,[2] Christian Sternemann,[2] and Roland Winter[1,*]
[1]Physical Chemistry I - Biophysical Chemistry, Faculty of Chemistry and Chemical Biology and [2]Fakultät Physik/DELTA, Technische Universität Dortmund, Dortmund, Germany

ABSTRACT For over 50 years, it has been known that the mitosis of eukaryotic cells is inhibited already at high hydrostatic pressure conditions of 30 MPa. This effect has been attributed to the disorganization of microtubules, the main component of the spindle apparatus. However, the structural details of the depolymerization and the origin of the pressure sensitivity have remained elusive. It has also been a puzzle how complex organisms could still successfully inhabit extreme high-pressure environments such as those encountered in the depth of oceans. We studied the pressure stability of microtubules at different structural levels and for distinct dynamic states using high-pressure Fourier-transform infrared spectroscopy and Synchrotron small-angle x-ray scattering. We show that microtubules are hardly stable under abyssal conditions, where pressures up to 100 MPa are reached. This high-pressure sensitivity can be mainly attributed to the internal voids and packing defects in the microtubules. In particular, we show that lateral and longitudinal contacts feature different pressure stabilities, and they define also the pressure stability of tubulin bundles. The intactness of both contact types is necessary for the functionality of microtubules in vivo. Despite being known to dynamically stabilize microtubules and prevent their depolymerization, we found that the anti-cancer drug taxol and the accessory protein MAP2c decrease the pressure stability of microtubule protofilaments. Moreover, we demonstrate that the cellular environment itself is a crowded place and accessory proteins can increase the pressure stability of microtubules and accelerate their otherwise highly pressure-sensitive de novo formation.

INTRODUCTION

Although they are exposed to extremes of temperature, pressure, pH, and salinity, a great variety of creatures can still be found living in regions characterized by these phenomena, which represent the greatest portion of our biosphere on Earth (1). Living systems, both prokaryotes and eukaryotes, are organized into highly dynamic and structured functional units, providing a platform for life. A dynamic and protein-composed cytoskeleton is required to spatiotemporally organize the cellular content, to establish cell shape, to provide mechanical strength, and to realize movement (2). It has been shown that such delicate tasks are among the most pressure-sensitive processes found in vivo (3–5). However, the underlying mechanism of the pronounced pressure sensitivity of the cytoskeleton is still largely unknown and is hence the focus of this work.

The eukaryotic cytoskeleton consists of four main kinds of filaments: actin filaments, microtubules, intermediate filaments, and septins (6). Among such non-covalently built-up biopolymers, microtubules are mainly involved in developing and maintaining cell shape and polarization and providing platforms for intracellular transport, and they are crucial for cell signaling and mitosis (2). To fulfill those functions, the heterodimer consisting of α- and β-tubulin ($\alpha\beta$-tubulin) polymerizes into hollow tubes of $\sim$25 nm in diameter, whereby the heterodimers form linear protofilaments in a head-to-tail fashion, and 10–15 of them then associate laterally to form a hollow and polar cylinder (7). Each tubulin monomer binds a guanine nucleotide, whereby the nucleotide bound to α-tubulin (N-site) is buried at the intradimer interface and is not hydrolyzed upon polymerization, whereas GTP bound to β-tubulin (E-site) is exchangeable in solution and becomes hydrolyzed in the polymerized state (7,8). Lateral interactions between protofilaments occur between adjacent α-tubulins and adjacent β-tubulins (homotypic contacts) forming a B-lattice with a seam in which α-tubulin and β-tubulin interact laterally (heterotypic contacts) (9,10).

Submitted November 10, 2017, and accepted for publication January 23, 2018.

*Correspondence: roland.winter@tu-dortmund.de

Editor: Andreas Engel.
https://doi.org/10.1016/j.bpj.2018.01.021

The microtubule assembly in vitro and in vivo is distinguished by the energetically unfavored and time-consuming nucleation step, which is bypassed in vivo by microtubule templates such as γ-tubulin ring complexes localized at the microtubule-organizing center (11,12). Spontaneous polymerization of tubulin in vitro requires a stable oligomer/nucleus consisting of several tubulin dimers (13). Once such nuclei are formed, they will elongate rapidly in both longitudinal and lateral direction (14). At steady state, microtubules undergo rapid cycles of growing and shrinking, a non-equilibrium behavior called dynamic instability (15), which is crucial for their cellular functions and is energetically realized by the polymerization-triggered hydrolysis of GTP bound to β-tubulin. A recent cryo-electron microscopy study revealed that the GTP hydrolysis provokes a lattice compaction around the interdimer interface along the protofilament axis, which is proposed to cause conformational strain that would be released by breaking of the lateral contacts and bending of the protofilaments during depolymerization (10,16,17). Interestingly, the structural compaction induced by GTP hydrolysis is inhibited in the presence of taxol, an antimitotic drug, which binds to a pocket in β-tubulin and is known to prevent microtubules from depolymerization (16,18).

In vivo, myriad microtubule-associated proteins (MAPs) are known to regulate the formation and the non-equilibrium dynamics of microtubules in a nucleotide-independent manner, mostly by stabilizing them against depolymerization (19). However, there are also MAPs (e.g., MCAK, Kip3p, and Kar3) known to destabilize microtubules, in particular by accumulating at the ends of growing microtubules, and thus to balance the growth and shrinkage required to regulate their dynamics (19,20). In case of stabilizing factors, MAPs like tau and MAP2 are also shown to be involved in inducing bundle formation of microtubules to grow and maintain membrane protrusions like axons and dendrites (21–23). Interestingly, such proteins do not directly cross-link the microtubules within the bundle, but control spacing between them by long-range repulsive forces reminiscent of polyelectrolyte polymer brushes (24). The C-terminal domain of such MAPs consists of three or four 18-residue microtubule binding repeats allowing electrostatic binding to the microtubule surface, whereby each repeat binds to one tubulin monomer, allowing longitudinal stabilization of microtubule protofilaments by bridging the interdimer interfaces (25). Furthermore, such abilities to bridge and shield charges have been reported to accelerate the steps of nucleation and elongation during microtubule formation (26–28). The N-terminal projection domain of MAPs varies in length for different isoforms and is highly negatively charged to keep microtubules at a distance from each other (29,30). However, the mechanism by which MAP2 and tau mediate attractive interactions between microtubules within bundles is largely unknown. Recently, the Safinya group proposed a mechanism by which the projection domains of tau on opposing microtubules mediate the spacing by a balance between repulsive forces and transient sub-k_BT cationic/anionic charge-charge attractions (22). In vitro, like-charge attraction between the negatively charged microtubules and formation of tightly packed hexagonal bundles have been observed in the presence of multivalent counterions (electrostatic condensation) and concentrated solutions of polymers (depletion attraction) (31–33).

Pioneering works in the 1960s to 1980s showed that elevated hydrostatic pressure induces mammalian epithelial cells to round up or marine eggs to arrest in the cell cycle, processes largely caused by disorganization of actin stress fibers and spindle microtubules, respectively (3–5). Pressures up to 30 MPa have been shown to induce rapid and reversible depolymerization of microtubules in a variety of eukaryotic cell types and thus to inhibit mitosis. However, details and the underlying mechanism of their pronounced pressure sensitivity are largely unknown. In contrast, actin filaments, another important component of the eukaryotic cytoskeleton, have been shown to be stable up to ~150–200 MPa (34,35). Recently, our laboratory showed that the pressure sensitivity of actin filaments originates from the limited pressure stability of the monomeric building block, which is hardly stable under abyssal conditions, and that actin-binding proteins such as cross-linkers and nucleators can significantly improve their pressure resistance (35–37). Here, we systematically studied the pressure stability of microtubules at different structural levels and for distinct dynamic states using high-pressure Fourier-transform infrared (FTIR) spectroscopy and Synchrotron small-angle x-ray scattering (SAXS). Our data provide structural details of the pressure-induced disintegration of microtubules and shed new light on molecular strategies to improve their pressure resistance.

MATERIALS AND METHODS

Reagents

$\alpha\beta$-Tubulin purified from calf brain was obtained from the Centre of Biological Research (CSIC; Madrid, Spain) as lyophilized powder. PIPES (1,4-piperazinediethanesulfonic acid), spermidine, and spermine were purchased from Sigma-Aldrich (Taufkirchen, Germany). Taxol from *Taxus brevifolia* was purchased from Sigma-Aldrich as dry powder and was dissolved in dimethylsulfoxide with a stock concentration of 2 mM.

Purification of MAP2c

Rat MAP2c was purified as described previously (38). Detailed methods can be found in the Supporting Material.

Sample preparation

Detailed methods for preparing dynamic and taxol-stabilized microtubules can be found in the Supporting Material.

High-pressure Synchrotron SAXS

SAXS experiments were performed at the beamline BL9 of DELTA in Dortmund, Germany (39), and the beamline I22 of the Diamond Light Source in Didcot, United Kingdom (40). Detailed methods can be found in the Supporting Material.

High-pressure FTIR

Pressure-dependent FTIR spectra were collected using a Nicolet 6700 FTIR spectrometer (Thermo Fisher Scientific, Waltham, MA) equipped with a liquid-nitrogen-cooled MCT detector (HgCdTe). Pressure up to 400 MPa was applied using a P-series diamond anvil cell (DAC) with type IIa diamonds (High Pressure Diamond Optics, Tucson, AZ). Detailed methods can be found in the Supporting Material.

Turbidimetry

High-pressure turbidimetry experiments were performed using a home-built pressure cell equipped with two sapphire windows. Detailed methods can be found in the Supporting Material.

Determination of void volumes

Void volumes are defined as water-inaccessible space inside proteins after removing all hetero atoms and were calculated using the CASTp server (41). Detailed methods can be found in the Supporting Material.

RESULTS

Stability of secondary structure

To explore the pressure stability of microtubules, we first examined the secondary structures of tubulin in distinct morphological states, as well as in the absence and presence of MAP2c, an isoform of MAP2 with a relatively short projection domain. To this end, the microtubules were polymerized in the presence of MAP2c at a 1:5 molar ratio of MAP2c to $\alpha\beta$-tubulin. Fig. 1 shows the pressure-dependent FTIR spectra of $\alpha\beta$-tubulin, microtubules, and MAP2c-bound microtubules. At ambient pressure, the area-normalized absorbance spectra of their amide I′ bands (1700–1600 cm^{-1}) are very similar in shape (Fig. 1, *A–C*). Only small differences are visible in the corresponding second-derivative spectra, which originate mainly from the different contents of secondary structure elements such as α-helices, β-sheets, turns, and random coils (Fig. 1, *D–F*) (42). Upon pressurization up to ~400 MPa, only marginal, but still significant, changes in spectral shape are visible, indicating no global unfolding of the protein. Conversely, high temperatures above 80°C lead to unfolding with subsequent aggregation, as indicated by the intermolecular β-sheet bands appearing at 1684 and 1618 cm^{-1} (Fig. 1, *G–I*). The second-derivative spectra of $\alpha\beta$-tubulin, microtubules, and MAP2c-bound microtubules reveal that the

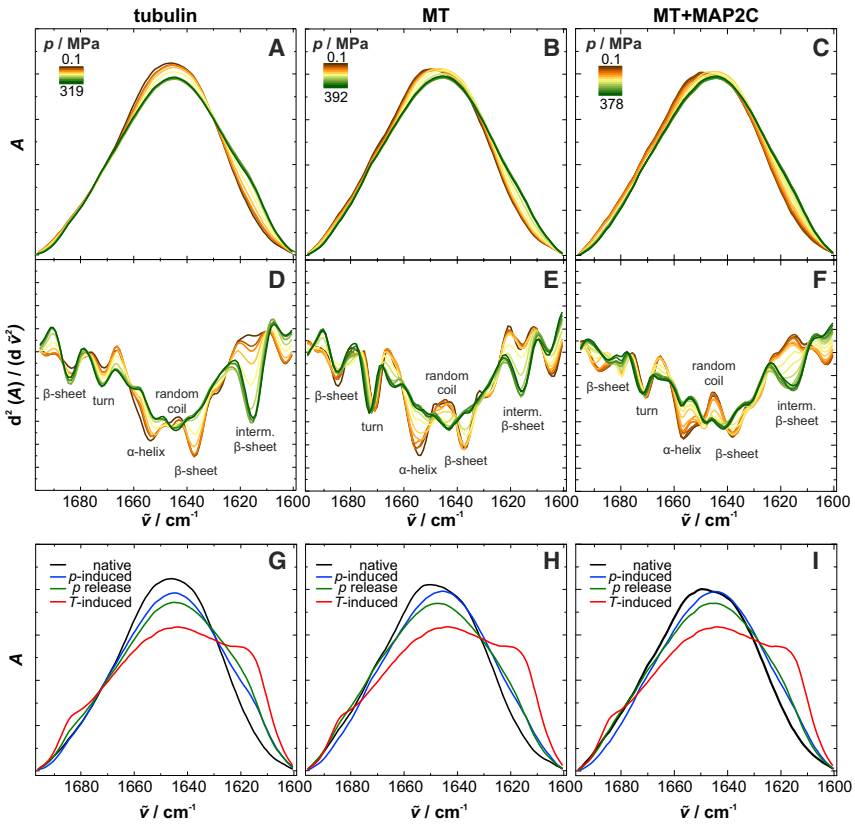

FIGURE 1 Effect of pressure on the secondary structure of microtubules in distinct morphological states. (*A–F*) Pressure-dependent normalized FTIR absorbance spectra (*A–C*) and second-derivative spectra (*D–F*) of the amide I′ band (1700–1600 cm^{-1}) for $\alpha\beta$-tubulin, microtubules, and MAP2c-bound microtubules at 37°C. (*G–I*) Temperature- and pressure-induced secondary structure changes are shown as normalized absorbance spectra. To see this figure in color, go online.

region most affected by pressure ranges from 1660 to 1630 cm^{-1}, which is assigned to α-helices, β-sheets, and random coils (Fig. 1, *D–F*). Pressure induces vanishing of the minima at 1653 and 1637 cm^{-1}, suggesting partial unwinding and unfolding of α-helices and intramolecular β-sheets. This is also consistent with the concomitant rise of the subband at 1644 cm^{-1}, which is assigned to random coils (43). In the case of $\alpha\beta$-tubulin and microtubules, the additional pressure-induced shift toward lower wavenumbers can be ascribed to enhanced exposure of such secondary structure elements to the solvent and thus toward strengthened hydrogen bonds between the backbone carbonyl groups and the solvent molecules (44). This observation might originate not only from partial unfolding, but also from disassembly of the heterodimers and microtubules leading to increased solvent-exposed secondary structure elements. By contrast, the presence of MAP2c causes a blue shift of such subbands, which can be ascribed to the pressure-induced elastic compression of chemical bonds (45). This indicates that those structural elements may interact with MAP2c and thus are shielded from the solvent, even upon a pressure increase up to ~400 MPa. The secondary structure of MAP2c itself is not affected by pressure in that range (Fig. S1). In contrast, the minima at 1684 and 1671 cm^{-1}, assigned to β-sheets and β-turns, shift slightly in all three cases to higher wavenumbers. Hence, those secondary structure elements are buried inside the protein and are hardly affected by pressure. However, the increase of the subband around 1616 cm^{-1} gives evidence of intermolecular β-sheet formation and thus partial aggregation induced by pressure (46), which is less pronounced compared to the thermally induced aggregation upon protein unfolding (Fig. 1, *G–I*).

Pressure effect on the quaternary structure

We performed complementary high-pressure Synchrotron SAXS studies to obtain structural information about the microtubules on the Ångstrom scale. Fig. 2, *A* and *B*, exhibits the pressure-dependent and background-subtracted SAXS intensity profiles of microtubules in the active (in the presence of excess GTP) and non-dynamic (stabilized by taxol) states, respectively. At atmospheric pressure, the shape of the scattering data is in both cases typical for the form factor of hollow cylinders (31). A qualitative fit shows that the active microtubules can be modeled as hollow cylinders with a wall thickness of 49 Å and an inner radius of 89–90 Å, which corresponds to the dimension of microtubules mainly consisting of 14 protofilaments (Fig. 2 *A*) (47). This is in agreement with literature data (7). In the case of the taxol-stabilized microtubules, the average inner radius is reduced to 84 Å when the wall thickness is kept constant (Fig. 2 *B*). This is also consistent with the observation that, in addition to stabilizing the existing population, taxol addition to preformed microtubules leads

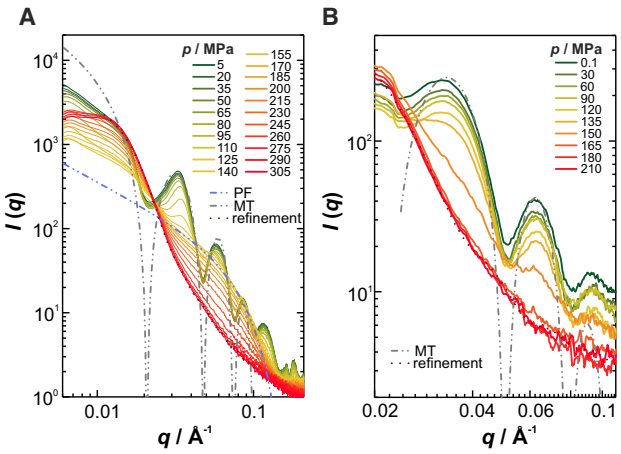

FIGURE 2 Effect of pressure on the quaternary structure of active and non-active microtubules. Pressure-dependent and azimuthally averaged Synchrotron SAXS data for (*A*) active microtubules at 37°C, and (*B*) taxol-stabilized microtubules at 25°C. The dotted lines show the fits for calculation of the pair-distance distribution function (refinement) (see the Supporting Material). The dash-dotted lines indicate the fitted model scattering curves for microtubules (*MT*) and protofilaments (*PF*) (see Results). To see this figure in color, go online.

to the appearance of 12-protofilament microtubules by decreasing the critical tubulin concentration for assembly (18,48,49). Upon pressurization, the intensity of the scattering maxima decreases, indicating disintegration of both microtubule species (Fig. 2). For the active microtubules, an intermediate species is observed at 155 MPa upon microtubule disintegration. Its scattering profile is characteristic of protofilaments, featuring a diameter of ~48 Å. Upon further compression up to 305 MPa, such protofilaments vanish and dissociate into oligomeric species. The pair-distance distribution function, $p(r)$, indicates a globular form for such oligomers with an average radius of gyration, R_g, of 130 Å (Fig. 2 *A*; Fig. S2). In contrast, pressure induces the taxol-stabilized and non-active microtubules to dissociate directly into oligomeric species with a smaller R_g value of 90 Å (Fig. 2 *B*; Fig. S2). At 150 MPa, the microtubules are completely dissociated, without forming an intermediate species. This finding suggests that binding to taxol destabilizes protofilaments against pressure and causes simultaneous disintegration of lateral and longitudinal contacts of microtubules.

Next, we tested whether MAP2c, known to longitudinally bridge tubulin subunits along the protofilaments, thereby inhibiting dynamic instability (25), is able to stabilize the longitudinal contacts of active microtubules against pressure (Fig. 3 *A*). At ambient conditions, the shape of the scattering pattern is entirely determined by the form factor of non-interacting microtubules, indicating that MAP2c does not induce formation of microtubule bundles as it does in vivo (21). However, the SAXS profile is shifted to lower q in the presence of MAP2c, indicating an increase of the radial size of microtubules (Fig. 3 *B*). Both an increased

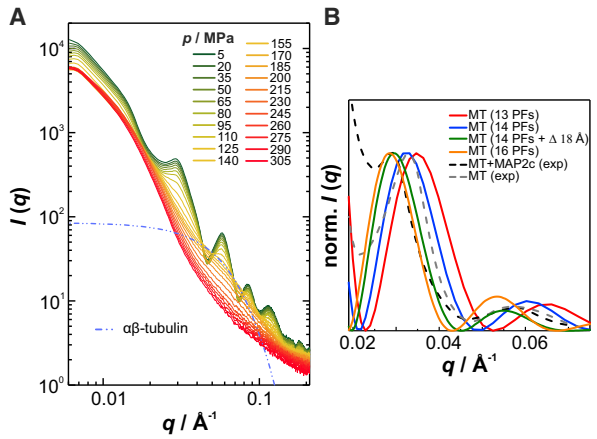

FIGURE 3 Effect of MAP2c on the pressure stability of active microtubules. (*A*) Pressure-dependent and azimuthally averaged Synchrotron SAXS data for active microtubules at 37°C and bound to MAP2c. The microtubules are polymerized in the presence of MAP2c with a 1:5 molar ratio of MAP2c to $\alpha\beta$-tubulin. The dash-dotted line shows the theoretical scattering profile of $\alpha\beta$-tubulin (PDB: 1JFF). (*B*) Comparison between experimental scattering profiles of active microtubules in the absence and presence of MAP2c and theoretical form factors of microtubules consisting of different numbers of protofilaments or featuring increased wall thickness. For better comparison, the scattering profiles are normalized to equal height of the first peak maxima. To see this figure in color, go online.

protofilament number and wall thickening due to MAP2c binding can contribute to the observed radial expansion of microtubules. Qualitative fits suggest that either the mean protofilament number is increased from 14 to 16 or MAP2c binding causes an 18-Å-thick layer on the microtubule surface (Fig. 3 *B*). As the contrast between the electron density in the region containing MAP2c and that of water is expected to be small (25,50), the latter scenario seems unlikely. Again, we found a simultaneous disintegration of lateral and longitudinal contacts upon pressurization, but with $\alpha\beta$-tubulin dimers as the dominating species at 155 MPa, which denature and vanish upon further compression up to 305 MPa (Fig. 3 *A*; Fig. S3). When starting from the unpolymerized state, a pressure-dependent behavior similar to that for $\alpha\beta$-tubulin is observed, although it exhibits less pressure stability (Fig. S3). Hence, binding to the longitudinal cross-linker does not improve, but rather impairs the pressure resistance of the microtubule's longitudinal organization.

Pressure stability of microtubule bundles

Further, we investigated the pressure stability of microtubule bundles, tubulin's next level of supramolecular self-assembly, whereby the like-charge attraction between the taxol-stabilized microtubules is induced either by electrostatic condensation or by depletion attraction. Multivalent cations such as spermidine (3+) and spermine (4+) have been reported to condense onto microtubules as polyanions, thereby partially neutralizing their charge and thus inducing attractive interaction between them (31). Depletion attraction can be found in crowded environments like those encountered in cells, where up to 40% of the cellular volume is occupied by different macromolecules (51). As the ensuing effect of excluded volume increases the osmotic pressure and entropy penalty (52), attractive forces between macromolecules such as microtubules are facilitated (32). To mimic the intracellular crowding density, polyethylene glycol (PEG) 20k was used as a crowding agent. Fig. 4 *A* shows that both electrostatic and depletion forces are able to induce the formation of microtubule bundles, which are packed into a hexagonal lattice, as indicated by the Bragg peak positions at q_{10}, $q_{11} = \sqrt{3}q_{10}$, $q_{20} = 2q_{10}$, $q_{21} = \sqrt{7}q_{10}$, $q_{30} = 3q_{10}$, and $q_{31} = \sqrt{13}q_{10}$, with a center-to-center distance of $a_H = 4\pi/(\sqrt{3}\,q_{10})$. Some diffraction peaks are not apparent due to the overlapping form factor minima of microtubules at those positions. The peak maxima at q_{11} and q_{21} were analyzed. In the case of the cations spermidine and spermine, the center-to-center distances amount to ~303 and 295 Å, whereas the presence of 10 and 20 wt % PEG 20k causes center-to-center distances of ~303 and 292 Å, respectively. Hence, the tightness of the hexagonal bundles increases with the valence of the counterion as well as the crowding density, findings that are consistent with literature data (31,32). When applying pressure, we observed a direct dissociation of all but the spermidine-induced bundles into denatured oligomers of tubulin, indicating that the pressure stability of the bundle phase is predominantly determined by the pressure limits of microtubules (Fig. 4, *C–E*). In the case of spermidine, pressurization up to 90 MPa induces a gradual dissociation of the bundles into individual microtubules, which then disintegrate completely at 150–165 MPa (Fig. 4 *B*). This can be explained by the weakening effect of pressure on electrostatic interactions (referred to as the electrostrictive effect), because dissociation of ion pairs results in rehydration of the ions, which is accompanied by formation of a compact hydration layer and thus reduction in the overall volume (53). Similar pressure sensitivity was recently observed for Mg^{2+}-induced actin filament bundles (36). In contrast, the charge density of the tetravalent cation spermine seems to be high enough to overcome the electrostrictive effect and maintain the electrostatic condensation of the microtubules up to 150–165 MPa, where pressure causes complete disintegration of taxol-stabilized microtubules. It is interesting to note that the crowding effect induced by PEG elevates the pressure stability of microtubules to 180–195 MPa.

Pressure sensitivity of microtubule polymerization kinetics

By performing pressure-dependent turbidimetric measurements at 37°C, we studied also the polymerization kinetics of microtubules as a function of pressure (Fig. 5). In

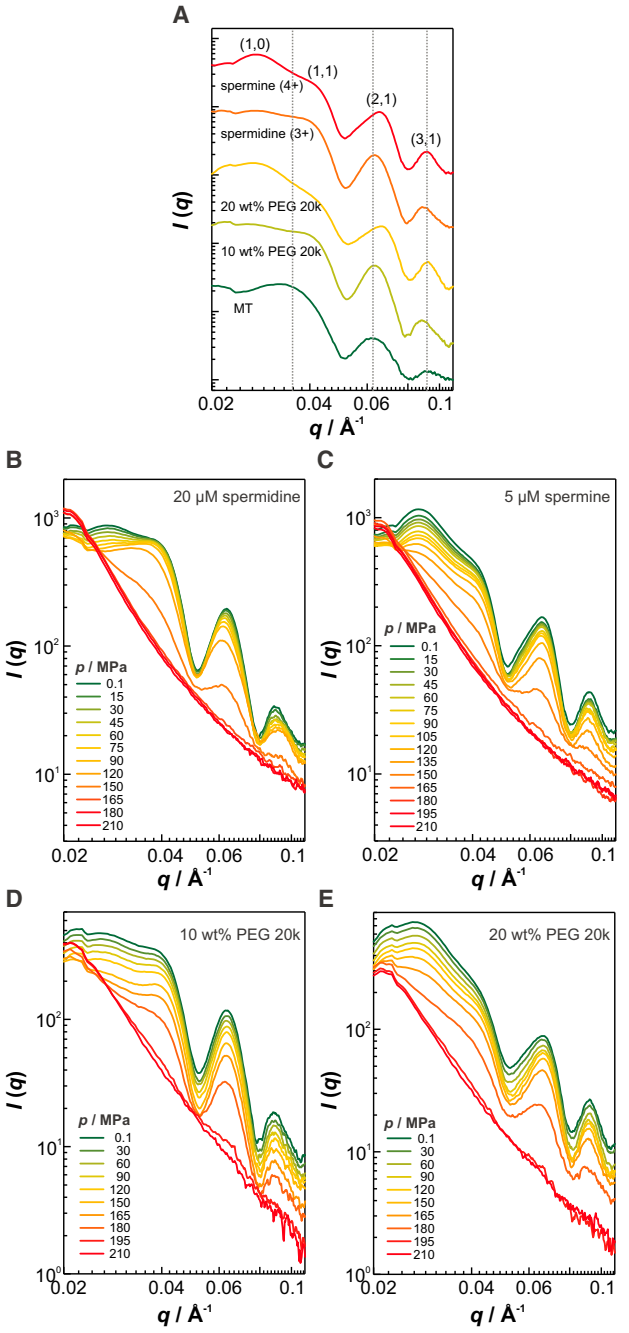

FIGURE 4 Pressure stability of microtubule bundles. (*A*) Synchrotron SAXS data of various bundle types of taxol-stabilized microtubules at 25°C and atmospheric pressure. (*B–E*) Pressure-dependent scattering profiles of microtubule bundles induced by (*B*) 20 μM spermidine, (*C*) 5 μM spermine, (*D*) 10 wt % PEG 20k, and (*E*) 20 wt % PEG 20k. To see this figure in color, go online.

addition, using MAP2c as a nucleator, we could bypass the initial nucleation step, allowing us to distinguish between the events of nucleation and elongation (Fig. 5 *A*). In the absence of MAP2c, a sigmoidal polymerization profile is observed, where small elongation-competent tubulin oligomers have first to be formed in the nucleation step for further lateral and longitudinal growth in the elongation phase (Fig. 5 *A*). The addition of MAP2c leads to the nucleation phase being bypassed, resulting in an exponentially shaped time course of polymerization (Fig. 5 *A*). Increasing pressure modulates the kinetics of the nucleation and elongation events differently (Fig. 5, *B–E*). Although the de novo polymerization of tubulin is already retarded at 60 MPa and nearly inhibited at 90 MPa within the measured time range (Fig. 5, *B* and *C*), the elongation kinetics is hardly affected by pressure up to 90 MPa (Fig. 5, *D* and *E*). Owing to the relatively high dead time of the high-pressure setup, the data are interpreted in a qualitative manner only. However, the pressure-dependent decrease of the plateau values of the unnormalized turbidimetry data in both cases indicates that smaller amounts and/or shorter microtubules are formed under high-pressure conditions. Formation of unusual assemblies like spirals, flat sheets, and other oligomers could also contribute to the reduced turbidity. Such findings render the initial oligomer formation the most pressure-sensitive process of microtubule formation.

DISCUSSION

According to Le Châtelier's principle, an increase of pressure shifts a chemical equilibrium toward conformations occupying smaller volumes, commonly realized by the release of defect volumes (packing defects) inside biomolecules or at intermolecular interfaces (54,55). Generally, a change in reaction volume can be described as the sum of intrinsic, thermal, and hydration contributions (56). The intrinsic volume consists of the van der Waals volume of the constituent atoms plus the volume of intrinsic voids, which are water inaccessible. The hydrational term describes, with regard to the bulk solvent, the solvent volume associated with the hydration of solvent-accessible atomic groups of the biomolecule. The thermal volume is caused by void volumes surrounding the solvent-accessible surface area (SASA) of the biomolecule and results from thermally induced mutual molecular vibrations and reorientations of the solute and the solvent. Unlike thermal unfolding, high pressures generally cause water penetration into the biomolecule's interior, resulting in filling of the voids and swelling of the core. In particular, pressure-induced unfolding of proteins is mainly determined by the presence of internal cavities and voids (57–59). To reveal the molecular origin of microtubule pressure sensitivity, we calculated the water-inaccessible voids (without mouth openings to the outside bulk solution) located inside microtubules based on cryo-electron microscopy structures using CASTp (41). We found significant voids in the tubulin subunits and packing defects at the contact sites along the protofilaments, whereas the lateral contacts between the protofilaments do not contribute to any significant defect volumes. Such interfilament contacts are only created by a single point, where a tyrosine or histidine residue of one subunit is sandwiched by

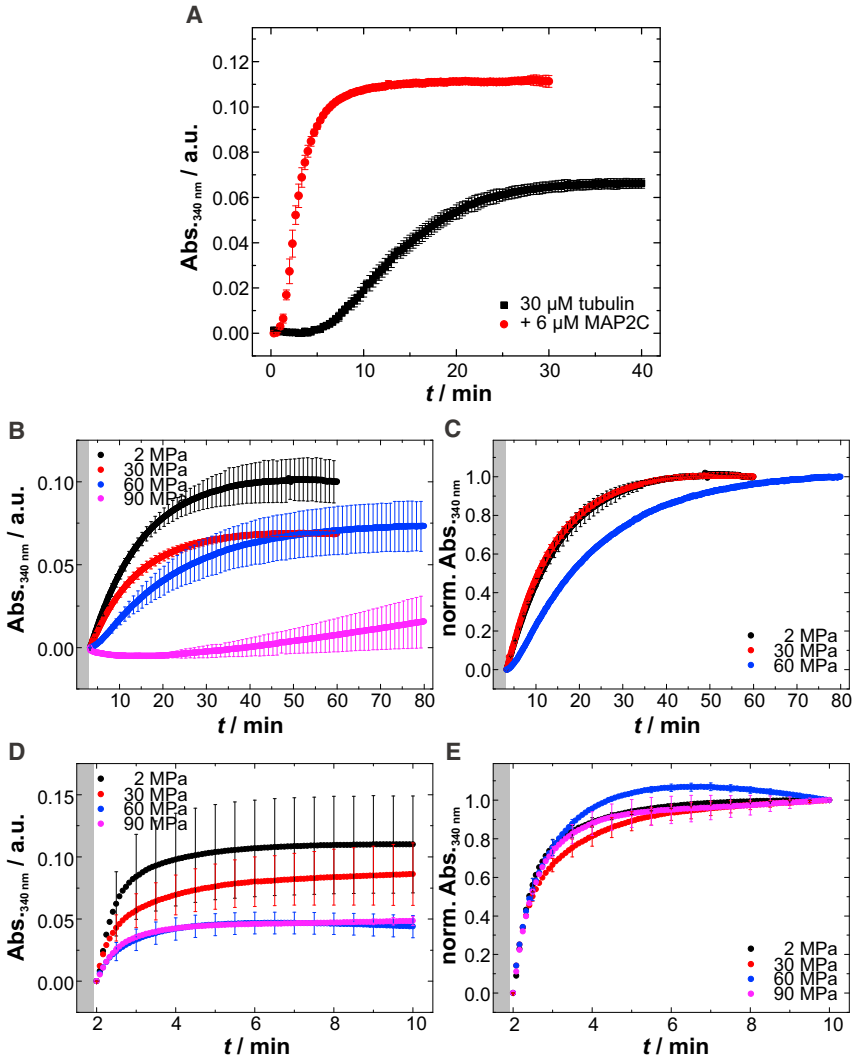

FIGURE 5 Pressure effect on the microtubule formation. (*A*) Effect of 6 μM MAP2c on the polymerization of 30 μM $\alpha\beta$-tubulin at 37°C and atmospheric pressure monitored by turbidimetry (at λ = 340 nm). (*B* and *D*) Pressure-dependent time course of the de novo polymerization and elongation of tubulin at 37°C and in the (*B*) absence and (*D*) presence of MAP2c. (*C* and *E*) For better comparison of the underlying kinetics, the normalized turbidimetry data corresponding to (*B*) and (*D*), respectively, are shown. To see this figure in color, go online.

two loops of the adjacent subunit, resembling a lock-and-key configuration (10). Despite a high degree of identity, α-tubulin shows increased internal void volumes compared to β-tubulin (Fig. 6 *A*). Notably, events like GTP hydrolysis and binding to taxol lead to an increase of voids within the α-subunit (Fig. 6 *C*). In contrast, packing defects along the protofilaments are more pronounced for the intradimer than for the interdimer interface (Fig. 6, *B* and *C*). Therefore, such voids and packing defects can significantly impair the stability of microtubules under high-pressure conditions.

Our results clearly show that the lateral contacts are the most pressure-sensitive interactions in active microtubules. The most likely explanation for this high-pressure sensitivity could be the fragile lock-and-key configuration forming the lateral contact, which may be susceptible to perturbation by the high local compressibilities of internal voids of the tubulin subunits. Thus, any minor structural change of this contact site, most likely induced by the partial unfolding and unwinding of secondary structure elements of tubulin, as observed by FTIR spectroscopy, can cause lateral dissociation of the microtubules into protofilaments. The subsequent disintegration of the protofilaments observed upon further pressurization can be interpreted as a consequence of release of packing defects at the longitudinal contact interfaces. This is further facilitated by the pressure-induced weakening of salt bridges and polar interactions, which are involved in forming the intra- and interdimer contacts (8). Another possibility is the release of the nucleotide at the E- and/or N-site, which has been demonstrated to cause disintegration of filaments formed by actin and its prokaryotic homolog ParM upon pressurization (34,60). In the case of taxol-stabilized microtubules, we found the pressure stability of the microtubule protofilaments to be decreased. Although taxol binds to a pocket in β-tubulin and restores the GDP lattice to a GTP-like extended state by swelling its binding site and expanding longitudinally the interdimer interface (16), our void analysis shows that taxol binding is also accompanied

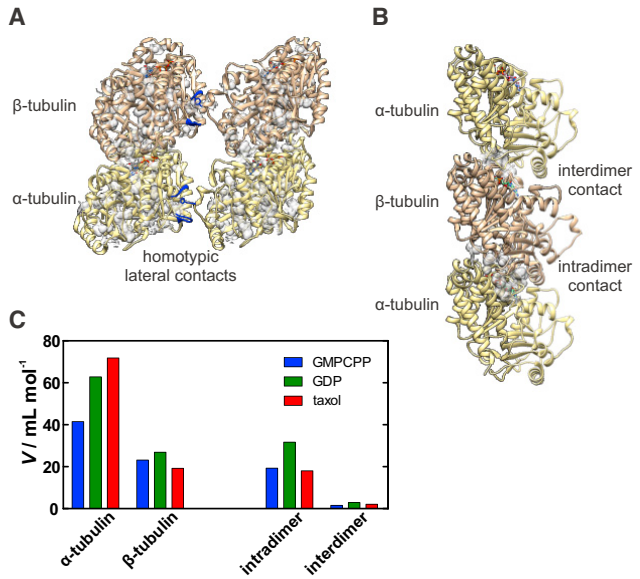

FIGURE 6 Water-inaccessible voids located in microtubules. A spherical probe for H_2O with a radius of 1.4 Å was used for the calculations. (*A*) Three-dimensional structure of the guanosine-5'-[(α,β)-methyleno]triphosphate (GMPCPP)-bound microtubule showing the voids (*gray*) located in the α- and β-subunits, as well as the homotypic lateral contacts (*blue*) between the protofilaments. (*B*) Packing defects (voids) formed at the inter- and intradimer contact sites along the protofilament. The images were prepared and modified with UCSF Chimera v1.11.2 using PDB: 3J6E. (*C*) Comparison of the total volumes of voids/packing defects within the subunits and at the contact sites of microtubules for the distinct chemical states produced by binding to GMPCPP, GDP, or taxol. To see this figure in color, go online.

by significantly increased formation of packing defects in α-tubulin (Fig. 6 *C*). This could explain the simultaneous dissociation of lateral and longitudinal contacts of taxol-bound microtubules under high-pressure conditions. In contrast to the case of taxol binding, the decreased pressure stability of protofilaments observed in the presence of MAP2c is more likely caused by additional packing defects at the longitudinal interfaces provoked by lattice constraints, which are a result of MAP2c acting on the protofilament conformation. These findings indicate that such longitudinal cross-linkers are not able to do double duty and that other molecular strategies are thus required to improve the pressure tolerance of microtubules in deep sea organisms. Interestingly, although taxol and MAP2c modulate the number of protofilaments and thus the lattice of microtubules, we did not find distinguishable pressure stabilities for lateral organization among the microtubule types.

Given the observed pressure sensitivity of the lateral and longitudinal contacts in microtubules, we found that they also determine the pressure stability of the bundle phase, which is in stark contrast to the effect of pressure on actin filament bundles. Recently, we reported that interfilament interactions between actin filaments realized by electrostatic condensation (induced by Mg^{2+}) and a protein cross-linker (fascin) are gradually diminished by pressure, leading to a decreasing tightness of the bundle phase and thus a continuously increasing interfilament distance before complete dissociation into actin filaments occurs (36). In the case of microtubule bundles, pressure does not modulate the packing tightness before complete disintegration of the bundles into denatured oligomers. Hence, actin filaments and microtubules, as the most important components of the eukaryotic cytoskeleton, exhibit not only differences in their morphology and function, but also in their pressure stability. At 150 MPa, the upper limit of the physiologically relevant pressure range, when the microtubules and their bundles are completely disintegrated, actin filaments start to deform, and their dissociation is completed only beyond 400 MPa (35). In contrast, cytoskeletal filaments formed by their prokaryotic homologs (e.g., FtsZ, MreB, and ParM) exhibit pressure tolerances ranging from 40 to 200 MPa (60–62).

Despite the high-pressure sensitivity of such cytoskeletal components, life has not been prevented from invading the high-pressure habitats of marine depths. This raises the question of which strategies deep sea organisms have evolutionarily established at a molecular level to improve the pressure resistance of their cytoskeleton. For microtubules, we found that the effect of macromolecular crowding, a typical generic phenomenon of the cellular environment, can increase the pressure stability of microtubules by 15–45 MPa. The high content of macromolecules inside cells restricts the accessible volume by the excluded volume effect (steric repulsion) and thus entropically stabilizes proteins and enhances their associations by favoring more compact and folded structures (63). In addition, we demonstrated that accessory proteins like MAP2c can also assist in ensuring the formation of microtubules under high-pressure stress, thereby acting as a nucleator to bypass the pressure-sensitive nucleation step, the initial event of tubulin self-assembly. The pressure-dependent retardation of the nucleation step corresponds to a positive activation volume, which reflects the formation of large defect volumes and the release of hydration water during the assembly of tubulin oligomers as elongation-competent nuclei. Similar observations were also made by us for the polymerization reaction of actin filaments (37,64).

CONCLUSIONS

We have investigated the pressure stability of microtubules in different dynamic states using FTIR spectroscopy and SAXS and discussed the origin of the observed pressure sensitivity. In summary, we showed that microtubules are hardly stable under abyssal conditions, where pressures up to at least 100 MPa are reached. We show that this pressure sensitivity can be mainly attributed to the internal voids and packing defects in the microtubules. Most importantly, we found that at every structural level, microtubules are less pressure stable compared to actin filaments. In particular,

we found that lateral and longitudinal contacts feature different pressure stabilities in the case of dynamic microtubules. The more pressure-labile lateral interactions cause a progressive disintegration of the microtubules into protofilaments upon pressurization. The longitudinal dissociation starts from 150 MPa. This is consistent with the in vivo observation that pressures up to 30 MPa induce rapid and reversible depolymerization of spindle microtubules in a variety of eukaryotic cell types and thus inhibit mitosis (3–5). Hence, the intactness of both contact types is necessary for the functionality of microtubules in vivo. Further, we showed that such contacts also define the pressure stability of the bundle phase. The dynamic instability of microtubules is commonly explained by thermodynamically labile associations of $\alpha\beta$-tubulin, in addition to conformational changes driven by GTP hydrolysis. Both taxol and MAP2c are known to bind to microtubules and prevent them from depolymerization. However, we found that the pressure instability of the contact sites does not correlate with the dynamics of microtubules. In contrast, binding to taxol or MAP2c causes a decreased pressure stability of the protofilaments relative to that of the active microtubule protofilaments. Hence, owing to the high-pressure sensitivity of the microtubules, adaptation strategies, both intrinsic and extrinsic, must exist in nature to improve the pressure resistance of cellular dynamics and movements found in living organisms thriving under extreme pressure conditions. In this study, we found that the cellular environment itself is a crowded place and that accessory proteins (e.g., MAP2c as nucleator) can increase the pressure stability of microtubules and accelerate their otherwise highly pressure-sensitive de novo formation. Further adaptation strategies need to be unraveled to fully understand how the range of extreme environments that organisms can successfully inhabit could expand.

SUPPORTING MATERIAL

Supporting Materials and Methods and three figures are available at http://www.biophysj.org/biophysj/supplemental/S0006-3495(18)30147-4.

AUTHOR CONTRIBUTIONS

M.G. and R.W. designed the research. M.G., M.B., S.M., N.E., and M.H. performed research. M.G. and R.W. analyzed data. V.S., C.S., and K.J. contributed analytic tools. M.G. and R.W. wrote the article. All authors discussed the results and commented on the manuscript.

ACKNOWLEDGMENTS

High-pressure Synchrotron SAXS experiments were performed on the beamline BL9 of DELTA in Dortmund, Germany, and the beamline I22 of the Diamond Light Source (DLS) in Didcot, United Kingdom. We are grateful to Andrew J. Smith at the DLS for providing assistance in using beamline I22. Further, we thank Steffen Bornemann, Mridula Dwivedi, Jan Latarius, and Lei Li for support at the beamlines and Jens Warmers (Max Planck Institute, Dortmund, Germany) for help with the electrospray ionization mass spectroscopy analysis. The pEGFP-N3_rMAP2c plasmid was a kind gift from Leif Dehmelt (Max Planck Institute, Dortmund, Germany).

Financial support from the Deutsches Forschungsgemeinschaft Research Unit FOR 1979, and in part from the Cluster of Excellence RESOLV (EXC 1069) and the Fonds der Chemischen Industrie, is gratefully acknowledged.

SUPPORTING CITATIONS

References (65–72) appear in the Supporting Material.

REFERENCES

1. Daniel, I., P. Oger, and R. Winter. 2006. Origins of life and biochemistry under high-pressure conditions. *Chem. Soc. Rev.* 35:858–875.
2. Fletcher, D. A., and R. D. Mullins. 2010. Cell mechanics and the cytoskeleton. *Nature.* 463:485–492.
3. Zimmerman, A. M., and D. Marsland. 1964. Cell division: effects of pressure on the mitotic mechanisms of marine eggs. *Exp. Cell Res.* 35:293–302.
4. Bourns, B., S. Franklin, …, E. D. Salmon. 1988. High hydrostatic pressure effects in vivo: changes in cell morphology, microtubule assembly, and actin organization. *Cell Motil. Cytoskeleton.* 10:380–390.
5. Salmon, E. D. 1975. Pressure-induced depolymerization of spindle microtubules. I. Changes in birefringence and spindle length. *J. Cell Biol.* 65:603–614.
6. Mostowy, S., and P. Cossart. 2012. Septins: the fourth component of the cytoskeleton. *Nat. Rev. Mol. Cell Biol.* 13:183–194.
7. Desai, A., and T. J. Mitchison. 1997. Microtubule polymerization dynamics. *Annu. Rev. Cell Dev. Biol.* 13:83–117.
8. Nogales, E., M. Whittaker, …, K. H. Downing. 1999. High-resolution model of the microtubule. *Cell.* 96:79–88.
9. Mandelkow, E. M., R. Schultheiss, …, E. Mandelkow. 1986. On the surface lattice of microtubules: helix starts, protofilament number, seam, and handedness. *J. Cell Biol.* 102:1067–1073.
10. Zhang, R., G. M. Alushin, …, E. Nogales. 2015. Mechanistic origin of microtubule dynamic instability and its modulation by EB proteins. *Cell.* 162:849–859.
11. Kollman, J. M., A. Merdes, …, D. A. Agard. 2011. Microtubule nucleation by γ-tubulin complexes. *Nat. Rev. Mol. Cell Biol.* 12:709–721.
12. Mitchison, T., and M. Kirschner. 1984. Microtubule assembly nucleated by isolated centrosomes. *Nature.* 312:232–237.
13. Job, D., O. Valiron, and B. Oakley. 2003. Microtubule nucleation. *Curr. Opin. Cell Biol.* 15:111–117.
14. Kerssemakers, J. W. J., E. L. Munteanu, …, M. Dogterom. 2006. Assembly dynamics of microtubules at molecular resolution. *Nature.* 442:709–712.
15. Mitchison, T., and M. Kirschner. 1984. Dynamic instability of microtubule growth. *Nature.* 312:237–242.
16. Alushin, G. M., G. C. Lander, …, E. Nogales. 2014. High-resolution microtubule structures reveal the structural transitions in $\alpha\beta$-tubulin upon GTP hydrolysis. *Cell.* 157:1117–1129.
17. Akhmanova, A., and M. O. Steinmetz. 2015. Control of microtubule organization and dynamics: two ends in the limelight. *Nat. Rev. Mol. Cell Biol.* 16:711–726.
18. Kellogg, E. H., N. M. A. Hejab, …, E. Nogales. 2017. Insights into the distinct mechanisms of action of taxane and non-taxane microtubule stabilizers from cryo-EM structures. *J. Mol. Biol.* 429:633–646.
19. Howard, J., and A. A. Hyman. 2007. Microtubule polymerases and depolymerases. *Curr. Opin. Cell Biol.* 19:31–35.

20. Akhmanova, A., and M. O. Steinmetz. 2008. Tracking the ends: a dynamic protein network controls the fate of microtubule tips. *Nat. Rev. Mol. Cell Biol.* 9:309–322.

21. Chen, J., Y. Kanai, …, N. Hirokawa. 1992. Projection domains of MAP2 and tau determine spacings between microtubules in dendrites and axons. *Nature.* 360:674–677.

22. Chung, P. J., C. Song, …, C. R. Safinya. 2016. Tau mediates microtubule bundle architectures mimicking fascicles of microtubules found in the axon initial segment. *Nat. Commun.* 7:12278.

23. Conde, C., and A. Cáceres. 2009. Microtubule assembly, organization and dynamics in axons and dendrites. *Nat. Rev. Neurosci.* 10:319–332.

24. Mukhopadhyay, R., and J. H. Hoh. 2001. AFM force measurements on microtubule-associated proteins: the projection domain exerts a long-range repulsive force. *FEBS Lett.* 505:374–378.

25. Al-Bassam, J., R. S. Ozer, …, R. A. Milligan. 2002. MAP2 and tau bind longitudinally along the outer ridges of microtubule protofilaments. *J. Cell Biol.* 157:1187–1196.

26. Cleveland, D. W., S. Y. Hwo, and M. W. Kirschner. 1977. Physical and chemical properties of purified tau factor and the role of tau in microtubule assembly. *J. Mol. Biol.* 116:227–247.

27. Drechsel, D. N., A. A. Hyman, …, M. W. Kirschner. 1992. Modulation of the dynamic instability of tubulin assembly by the microtubule-associated protein tau. *Mol. Biol. Cell.* 3:1141–1154.

28. Wolff, J., L. Knipling, and D. L. Sackett. 1996. Charge-shielding and the "paradoxical" stimulation of tubulin polymerization by guanidine hydrochloride. *Biochemistry.* 35:5910–5920.

29. Dehmelt, L., and S. Halpain. 2005. The MAP2/Tau family of microtubule-associated proteins. *Genome Biol.* 6:204.

30. Lewis, S. A., D. H. Wang, and N. J. Cowan. 1988. Microtubule-associated protein MAP2 shares a microtubule binding motif with tau protein. *Science.* 242:936–939.

31. Needleman, D. J., M. A. Ojeda-Lopez, …, C. R. Safinya. 2004. Higher-order assembly of microtubules by counterions: from hexagonal bundles to living necklaces. *Proc. Natl. Acad. Sci. USA.* 101:16099–16103.

32. Needleman, D. J., M. A. Ojeda-Lopez, …, C. R. Safinya. 2004. Synchrotron x-ray diffraction study of microtubules buckling and bundling under osmotic stress: a probe of interprotofilament interactions. *Phys. Rev. Lett.* 93:198104.

33. Asakura, S., and F. Oosawa. 1958. Interaction between particles suspended in solutions of macromolecules. *J. Polym. Sci.* 33:183–192.

34. Ikeuchi, Y., A. Suzuki, …, C. Balny. 2002. Fluorescence study of the high pressure-induced denaturation of skeletal muscle actin. *Eur. J. Biochem.* 269:364–371.

35. Rosin, C., M. Erlkamp, …, R. Winter. 2014. Exploring the stability limits of actin and its suprastructures. *Biophys. J.* 107:2982–2992.

36. Gao, M., M. Berghaus, …, R. Winter. 2015. Condensation agents determine the temperature-pressure stability of F-actin bundles. *Angew. Chem. Int.Engl.* 54:11088–11092.

37. Gao, M., and R. Winter. 2015. Kinetic insights into the elongation reaction of actin filaments as a function of temperature, pressure and macromolecular crowding. *ChemPhysChem.* 16:3681–3686.

38. Gamblin, T. C., K. Nachmanoff, …, R. C. Williams, Jr. 1996. Recombinant microtubule-associated protein 2c reduces the dynamic instability of individual microtubules. *Biochemistry.* 35:12576–12586.

39. Krywka, C., C. Sternemann, …, M. Tolan. 2007. The small-angle and wide-angle x-ray scattering set-up at beamline BL9 of DELTA. *J. Synchrotron Radiat.* 14:244–251.

40. Brooks, N. J., B. L. L. E. Gauthe, …, J. M. Seddon. 2010. Automated high pressure cell for pressure jump x-ray diffraction. *Rev. Sci. Instrum.* 81:064103.

41. Binkowski, T. A., S. Naghibzadeh, and J. Liang. 2003. CASTp: computed atlas of surface topography of proteins. *Nucleic Acids Res.* 31:3352–3355.

42. de Pereda, J. M., D. Leynadier, …, J. M. Andreu. 1996. Tubulin secondary structure analysis, limited proteolysis sites, and homology to FtsZ. *Biochemistry.* 35:14203–14215.

43. Prigozhin, M. B., Y. Liu, …, M. Gruebele. 2013. Misplaced helix slows down ultrafast pressure-jump protein folding. *Proc. Natl. Acad. Sci. USA.* 110:8087–8092.

44. Parrish, J. R., Jr., and E. R. Blout. 1972. The conformation of poly-L-alanine in hexafluoroisopropanol. *Biopolymers.* 11:1001–1020.

45. Smeller, L., F. Meersman, …, K. Heremans. 2003. High-pressure FTIR study of the stability of horseradish peroxidase. Effect of heme substitution, ligand binding, Ca++ removal, and reduction of the disulfide bonds. *Biochemistry.* 42:553–561.

46. Zandomeneghi, G., M. R. H. Krebs, …, M. Fändrich. 2004. FTIR reveals structural differences between native β-sheet proteins and amyloid fibrils. *Protein Sci.* 13:3314–3321.

47. Raviv, U., T. Nguyen, …, C. R. Safinya. 2007. Microtubule protofilament number is modulated in a stepwise fashion by the charge density of an enveloping layer. *Biophys. J.* 92:278–287.

48. Díaz, J. F., J. M. Valpuesta, …, J. M. Andreu. 1998. Changes in microtubule protofilament number induced by Taxol binding to an easily accessible site. Internal microtubule dynamics. *J. Biol. Chem.* 273:33803–33810.

49. Arnal, I., and R. H. Wade. 1995. How does taxol stabilize microtubules? *Curr. Biol.* 5:900–908.

50. Choi, M. C., U. Raviv, …, C. R. Safinya. 2009. Human microtubule-associated-protein tau regulates the number of protofilaments in microtubules: a synchrotron x-ray scattering study. *Biophys. J.* 97:519–527.

51. Ellis, R. J., and A. P. Minton. 2003. Cell biology: join the crowd. *Nature.* 425:27–28.

52. Marenduzzo, D., K. Finan, and P. R. Cook. 2006. The depletion attraction: an underappreciated force driving cellular organization. *J. Cell Biol.* 175:681–686.

53. Boonyaratanakornkit, B. B., C. B. Park, and D. S. Clark. 2002. Pressure effects on intra- and intermolecular interactions within proteins. *Biochim. Biophys. Acta.* 1595:235–249.

54. Meersman, F., I. Daniel, …, P. F. McMillan. 2013. High-pressure biochemistry and biophysics. *Rev. Mineral. Geochem.* 75:607–648.

55. Silva, J. L., A. C. Oliveira, …, D. Foguel. 2014. High-pressure chemical biology and biotechnology. *Chem. Rev.* 114:7239–7267.

56. Gao, M., C. Held, …, R. Winter. 2017. Crowders and cosolvents-major contributors to the cellular milieu and efficient means to counteract environmental stresses. *ChemPhysChem.* 18:2951–2972.

57. Roche, J., J. A. Caro, …, C. A. Royer. 2012. Cavities determine the pressure unfolding of proteins. *Proc. Natl. Acad. Sci. USA.* 109:6945–6950.

58. Chen, C. R., and G. I. Makhatadze. 2017. Molecular determinant of the effects of hydrostatic pressure on protein folding stability. *Nat. Commun.* 8:14561.

59. Collins, M. D., G. Hummer, …, S. M. Gruner. 2005. Cooperative water filling of a nonpolar protein cavity observed by high-pressure crystallography and simulation. *Proc. Natl. Acad. Sci. USA.* 102:16668–16671.

60. Popp, D., A. Narita, …, Y. Maéda. 2008. Molecular structure of the ParM polymer and the mechanism leading to its nucleotide-driven dynamic instability. *EMBO J.* 27:570–579.

61. Popp, D., A. Narita, …, R. C. Robinson. 2010. Filament structure, organization, and dynamics in MreB sheets. *J. Biol. Chem.* 285:15858–15865.

62. Ishii, A., T. Sato, …, C. Kato. 2004. Effects of high hydrostatic pressure on bacterial cytoskeleton FtsZ polymers in vivo and in vitro. *Microbiology.* 150:1965–1972.

63. Zhou, H.-X., G. Rivas, and A. P. Minton. 2008. Macromolecular crowding and confinement: biochemical, biophysical, and potential physiological consequences. *Annu. Rev. Biophys.* 37:375–397.

64. Rosin, C., K. Estel, …, R. Winter. 2015. Combined effects of temperature, pressure, and co-solvents on the polymerization kinetics of actin. *ChemPhysChem.* 16:1379–1385.

65. Doll, T., A. Papandrikopoulou, and A. Matus. 1990. Nucleotide and amino acid sequences of embryonic rat MAP2c. *Nucleic Acids Res.* 18:361.

66. Basham, M., J. Filik, …, A. W. Ashton. 2015. Data analysis workbeNch (DAWN). *J. Synchrotron Radiat.* 22:853–858.

67. Hammersley, A. P., S. O. Svensson, and A. Thompson. 1994. Calibration and correction of spatial distortions in 2D detector systems. *Nucl. Instrum. Methods Phys. Res. A.* 346:312–321.

68. Sztucki, M., and T. Narayanan. 2007. Development of an ultra-small-angle x-ray scattering instrument for probing the microstructure and the dynamics of soft matter. *J. Appl. Cryst.* 40:s459–s462.

69. Breßler, I., J. Kohlbrecher, and A. F. Thünemann. 2015. SASfit: a tool for small-angle scattering data analysis using a library of analytical expressions. *J. Appl. Cryst.* 48:1587–1598.

70. Franke, D., M. V. Petoukhov, …, D. I. Svergun. 2017. ATSAS 2.8: a comprehensive data analysis suite for small-angle scattering from macromolecular solutions. *J. Appl. Cryst.* 50:1212–1225.

71. Wong, P. T. T., and D. J. Moffatt. 1989. A new internal pressure calibrant for high-pressure infrared spectroscopy of aqueous systems. *Appl. Spectrosc.* 43:1279–1281.

72. Pettersen, E. F., T. D. Goddard, …, T. E. Ferrin. 2004. UCSF Chimera—a visualization system for exploratory research and analysis. *J. Comput. Chem.* 25:1605–1612.